

CI Cam: A Shell-shocked X-ray Nova

Amy J. Mioduszewski^{1,2}
amiodusz@nrao.edu

Michael P. Rupen²
mrupen@nrao.edu

ABSTRACT

We present radio imaging observations of the 1998 outburst of the peculiar emission line star CI Cam, taken $\sim 1, 4, 75, 82, 93, 163,$ and 306 days after the beginning of the 31.64 March 1998 X-ray flare. The first two epochs show a resolved but compact (no larger than 12 milliarcseconds) radio source which becomes optically thin at frequencies higher than 5 GHz. The spectrum and brightness temperatures are consistent with synchrotron self-absorption, although free-free absorption may also play a role. The later images show a large (120 - 350 milliarcseconds) oval-shaped or double ring remnant. The radio spectrum combined with the high brightness temperature indicates that the emission is synchrotron, while the morphology suggests that this is powered by a decelerating shock moving through dense circumstellar material produced by a strong stellar wind. The radio images of CI Cam are equally well fit by an expanding ellipsoid or two expanding rings; the former gives $\Theta \approx 4.2(t - 50904.1)^{0.77}$, with Θ the major axis in mas and t the Modified Julian Date (MJD). The corresponding expansion speed in the plane of the sky was $\sim 12,000$ km/s over the first few days (for an assumed distance of 5 kpc), slowing by a factor ~ 3 by the time of the last observation almost a year later. The radio emission from all other X-ray binary transients has either been unresolved, or taken the form of highly collimated relativistic jets. We suggest that CI Cam represents a rare case where these jets were smothered early on by the unusually dense circumstellar medium. In this model CI Cam is the analogue to extragalactic supernovae formed by the collapsar mechanism, while the more usual X-ray binaries with relativistic jets are analogous to the jets which escape those supernovae to form a subset of γ -ray bursts.

Subject headings: binaries: close – stars: individual: CI Cam – radio continuum: stars – stars: flare – X-rays: binaries – X-rays: bursts

1. Introduction

XTE J0421+560 was discovered by the All-Sky Monitor (ASM) on the Rossi X-ray Timing Explorer (RXTE) on 31.64 March 1998 (Smith et al. 1998) as the first bright X-ray transient in several years, reaching almost 2 Crabs within a day of the first detection. Corresponding radio emission was detected soon after (1.9 April; Hjellming &

Mioduszewski 1998). Optical observations (Wagner & Starrfield 1998) identified the radio and X-ray transient as the star CI Cam, based on positional coincidence with the radio emission, and a concurrent optical outburst. It was also detected by the Burst and Transient Source Experiment in the low-energy Gamma-rays, reaching a flux of 1.6 mCrab in the 20 – 40 keV band (Harmon et al. 2004).

CI Cam is a peculiar bright emission-line star with unusually strong Fe II lines (Downes 1984), indicating a very hot star or stellar shell. It also

¹JIVE, Postbus 2, 7990 AA, Dwingeloo, the Netherlands

²NRAO, P.O. Box 0, Socorro, NM 87801, USA

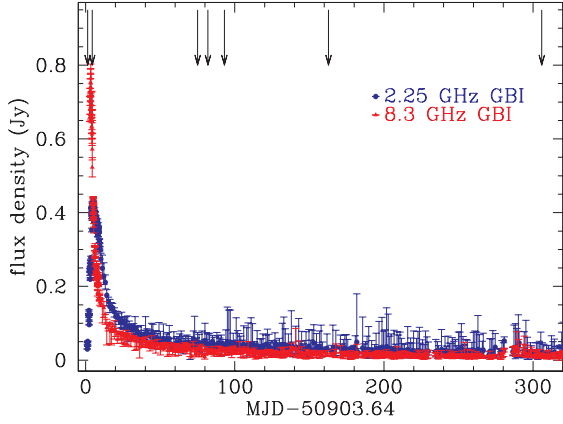


Fig. 1.— The radio light curve from the Green Bank Interferometer (GBI), as produced by R.M. Hjellming (priv. comm.). The green triangles and red circles represent 8.3 GHz and 2.25 GHz data respectively. After day 10 the data are averaged over 1 day and the error bars are the minimum and maximum for that day. The arrows show the epochs of our 7 imaging observations.

has a near-IR excess (Dong & Hu 1991; Allen & Swings 1976). CICam has a rich and unusual optical spectrum and has been identified as a symbiotic star (Chkhikvadze 1970), a Herbig Be star (Thé, de Winter, & Pérez 1994), a B[e] star (Belloni et al. 1999), and a supergiant B[e] (sgB[e]) star (Robinson, Ivans, & Welsh 2002; Hynes et al. 2002). The recent consensus seems to be that it is either a B[e] or sgB[e] star. If it is an sgB[e] star it would be the only one identified in our Galaxy, all others having been found in the Magellanic Clouds. Its distance has been estimated to be anything from 1 kpc (Chkhikvadze 1970) to 8 kpc (e.g., Robinson, Ivans, & Welsh 2002) based on luminosity, spectrum, interstellar absorption, and kinematics. Here we take 5 kpc as a reasonable compromise. CICam was not previously a known radio source, with two 10.7 GHz observations in 1973 giving upper limits of 5 mJy (Altenhoff, Braes, Olon, & Wendker 1976; Woodsworth & Hughes 1977).

CICam’s X-ray/radio/optical flare puts it into another class, that of X-ray novae. If CICam is at a distance greater than 2 kpc then its X-ray luminosity indicates that there is probably a compact object (black hole or neutron star) in the

system (e.g., Belloni et al. 1999). Orlandini et al. (2000) suggests that the outburst was the result of thermonuclear runaway on the surface of a white dwarf, which would require a closer distance. Even with all the different stellar identifications for the optical source, it is clear that CICam must be a high mass X-ray binary (HMXB). However, CICam’s X-ray behavior is unique among X-ray binaries. For instance, unlike other HMXBs, CICam does not have persistent highly variable X-ray emission, and has a soft X-ray excess in quiescence (Robinson, Ivans, & Welsh 2002). The persistent soft X-ray emission can be attributed to the sgB[e] star and the heavily absorbed harder emission may be an obscured compact object, but this is not certain, since this type of emission is extremely unusual for X-ray transients (Robinson, Ivans, & Welsh 2002). The flare itself peaked first in the X-ray, then in the optical, and finally at radio wavelengths (Frontera et al. 1998), with several short, soft X-ray flares within ten days of the outburst (Frontera et al. 1998; Ueda et al. 1998), and rapid changes in the X-ray absorption column over the first few days (Belloni et al. 1999), as well as years afterwards (Parmar et al. 2000). The radio behavior is fairly typical of X-ray transients, with an optically thick rise followed by an optically thin decay (Clark et al. 2000), but with no sign of further flaring activity. An initial report of a relativistic radio jet (Hjellming & Mioduszewski 1998) has since been shown to be an artifact due to a bad calibrator (Rupen, Mioduszewski, & Hjellming 2003).

In this paper we present a radio imaging study of CICam from a few days to roughly a year after the X-ray outburst, using the National Radio Astronomy Observatory’s (NRAO) Very Long Baseline Array (VLBA) and the United Kingdom national facility Multi-Element Radio Linked Interferometer Network (MERLIN).

2. Observations

CICam was observed on 1 April, 5 April, 14 June, 21 June, 2 July and 10 September 1998 with the full 10-element VLBA with the addition of one antenna of the Very Large Array (VLA), except for the 5 April 1998 observation, which was missing the Pie Town, Kitt Peak, and Owens Valley VLBA antennas. All of these observations

TABLE 1
OBSERVATIONS

MJD ^a	Epoch date	days since detection of X-ray flare ^b	antennas	freq. (GHz)	time on CI Cam (hours)	int. flux density (mJy)	rms (mJy/beam)
50904.92	1 Apr. 98	1.28	VLBA	1.667	2.8	3.6 ^c	0.23 ^c
50908.04	5 Apr. 98	4.4	BR FD HN LA MK NL SC Y1	1.667	2.1	221.7	0.28
50908.04	5 Apr. 98	4.4	BR FD HN LA MK NL SC Y1	4.987	2.0	524.6	0.59
50908.04	5 Apr. 98	4.4	BR FD HN LA MK NL SC Y1	15.37	1.9	190.6	0.53
50978.74	14 June 98	75.1	VLBA +Y1	1.667	1.7	41.5	0.085
50985.61	21 June 98	82.0	VLBA +Y1	1.667	1.7	39.3	0.086
	June 98 combined ^d	~79	VLBA +Y1	1.667	3.4	40.3	0.075
50996.65	2 July 98	93.0	VLBA +Y1	1.667	2.1	36.1	0.084
51066.45	10 Sep. 98	162.8	VLBA +Y1	1.667	6.8	20.0	0.036
51209.44	31 Jan. 99	305.8	MERLIN	4.994	10.0	4.3	0.15

^aModified Julian Date (Julian Date - 2400000.5) at mid-point of observations

^bThe X-ray flare was first detected on 31.64 March 1998 (MJD 50903.64), and peaked on 1.04 April 1998 (MJD 50904.04).

^cFlux densities for 1 April 98 data after correction for the primary beam, since the VLBA was pointed 11.4 arcminutes from the correct position.

^d14 June 98 + 21 June 98 data

NOTE.—VLBA antennas: BR-Brewster, FD-Fort Davis, HN-Hancock, KP-Kitt Peak, LA-Los Alamos, MK-Mauna Kea, NL-North Liberty, OV-Owens Valley, PT-Pie Town and SC-Saint Croix; Y1 - one VLA antenna; MERLIN antennas: Mark 2 (at Jodrell Bank), Cambridge, Defford, Knocking, Darnhall, and Tabley.

were carried out using left and right circular feeds with a bandwidth of 32 MHz in each polarization centered on 1.7 GHz, except for 5 April 1998, which used three bands centered on 1.7, 5.0 and 15.4 GHz. MERLIN, a 6 element interferometer in Great Britain, observed on 31 January 1999 at 5.0 GHz, with a bandwidth of 16 MHz in each polarization, again using circular feeds. Table 1 summarizes these observations. The VLBA observations were correlated at the VLBA correlator in Socorro, NM. Figure 1 shows the epochs of the VLBA observations in the context of the radio light-curves, taken from the Green Bank Interferometer (GBI) (Rupen et al., in prep.; see also Clark et al. 2000). The radio spectrum evolves smoothly from optically thick ($\alpha \sim 0.85$, $S_\nu \propto \nu^\alpha$) two days after the X-ray peak, to optically thin ($\alpha \sim -0.4$) synchrotron radiation, 7 days after the X-ray peak. CI Cam's radio emission is also, for X-ray novae, unusually long-lived, allowing it to be observed many months after the X-ray flare. The lack of secondary radio flares, in contrast to most other X-ray novae, allows a direct link between the radio remnant and the original impulsive event. CI Cam is in fact still detected (2004) at the ~ 1 mJy level with the VLA (Rupen et al., in prep).

All the VLBA observations were phase referenced to the strong VLBI sources J0419+5722 and J0422+5324, while the MERLIN experiment was only referenced to J0419+5722. Both of these sources are less than 1°5 away from CI Cam

and are excellent calibrators. For the VLBA observations we used a cycle time of 1 minute on J0419+5722, 2.5 minutes on CI Cam, then 1 minute on J0422+5324. The observations were reduced in the standard manner using the NRAO's Astronomical Image Processing System (Greisen 2003). The second epoch was phase and amplitude self-calibrated, but all other epochs were not. During the epoch the total flux smoothly varied by 10% in the 1.7 and 5.0 GHz and 20% in the 15.4 GHz data. The variations were flattened by the amplitude self-calibration and did not affect the structures in the images. The two June epochs were concatenated and imaged together. CI Cam evolves slowly enough that this is valid, and it improved the image considerably. On 1 April the VLBA observed the estimated X-ray position, which was off by 11.4 arcminutes. CI Cam was thus at the $\sim 60\%$ power point of the VLBA antennas at 1.7 GHz, so all flux densities for that date have been multiplied by 1.7. Since these observations were phase referenced the relative positions between the high frequency the maps are accurate, although the relative positions of the 1.7 GHz maps may differ by up to a few milliarcseconds (mas) due to the ionosphere. Also note that in these images 1 mas = $5 d_{5kpc}$ AU ($d_{5kpc} = d/5$ kpc, with d the distance to the source). A careful polarization calibration was not done, however we can say that CI Cam is not polarized by more than a few percent in any epoch, probably less than that for the second epoch.

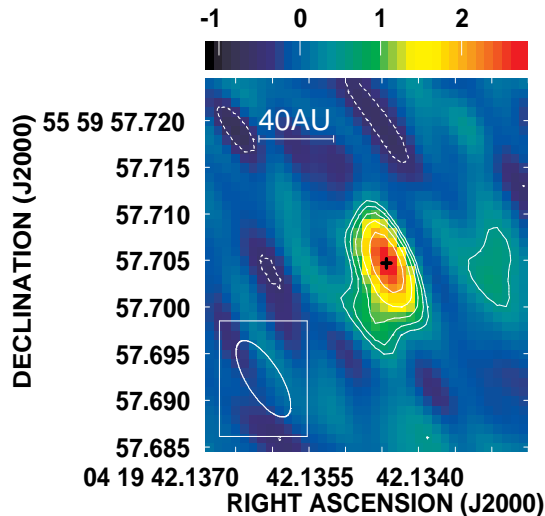


Fig. 2.— VLBA 1.7 GHz image of CICam on 1 April 1998, less than a day after the X-ray flare. Peak flux density 2.77 mJy/beam (3.3×10^7 K); beam size 9.61×3.80 mas at $34^\circ 5'$; rms noise 0.23 mJy/beam; contours at $\pm 2^{n/2} \times 0.5$ mJy/beam, $n = 0, 1, \dots, 4$; conversion to brightness temperature: 12×10^6 K/mJy/beam.

3. Images

3.1. April 1998

Figures 2 and 3 show the images from the first and second epochs. On 1 April 1998, during the radio rise, the source was very faint, and still optically thick at 1.7 GHz (see Figure 1). The map shows a peak of 2 mJy/beam; the faint extension to the southeast (Figure 2) is probably a noise spike. CICam may be slightly resolved (4 ± 2 mas) along a position angle of $\sim 20^\circ$, but this is very close to the position angle of the beam ($\sim 34^\circ 5'$), and so may not be real. By 5 April the turnover frequency between optically thick and optically thin emission was about 5 GHz, and the images (Figure 3) show a much more complicated structure. At 1.7 GHz, the source is resolved but very smooth, extending ~ 12 mas in the north-south direction. At optically thin frequencies, 5 and 15 GHz, CICam breaks up into several condensations with a “kidney-shaped” structure to the south.

3.1.1. Spectral Indices

There are significant differences between the images made at different frequencies on 5 April 1998: the 1.7 GHz image extends further north than the 5 and 15 GHz images would lead one to expect, while the western arm of the structure seen at 5 GHz is not present in the 15 GHz image. Some of these differences could easily be instrumental. Interferometers act as spatial filters, effectively measuring different components in the Fourier transform of the image. The Fourier component seen by a single baseline of length B corresponds to a spatial frequency of B/λ . Thus long baselines measure rapid fluctuations of the sky brightness, while short baselines respond to more gradual changes. The same physical interferometer, used at two different wavelengths, may respond quite differently to the identical source structure. High-resolution interferometric images for instance may not recover large-scale structures which contain most of the source flux density: one sees the crests of the waves, but not the ocean on which they rest. For more information see Taylor, Carilli, & Perley (1999) or Thompson, Moran, & Swenson (2001).

For CICam on 5 April 1998, the 5 GHz VLBA image recovers $\sim 94\%$ of the integrated flux density as measured by the VLA; while at 15 GHz the VLBA recovers only $\sim 47\%$ of that integrated flux density. This strongly suggests that at least part of the 5 GHz structure which is missing from the 15 GHz image has been removed by the more extensive spatial filtering operating at 15 GHz. To test this idea we put the CLEAN component model¹ of the 5 GHz data through the (u, v) (Fourier) coverage at 15 GHz, to simulate what the 5 GHz source would look like if observed at 15 GHz. This produces an image with a morphology almost identical to that actually observed at 15 GHz (see Figure 4), and with a total flux which is 50% less than the same area in the 5 GHz image (i.e., not including the western arm). In other words, even if its intrinsic structure were identical to that seen in the 5 GHz image, the 15 GHz image would not show the western arm because of the spatial filtering of the 15 GHz ob-

¹CLEAN is a deconvolution algorithm which models the emission as a set of point sources; see, e.g., Cornwell (Braun).

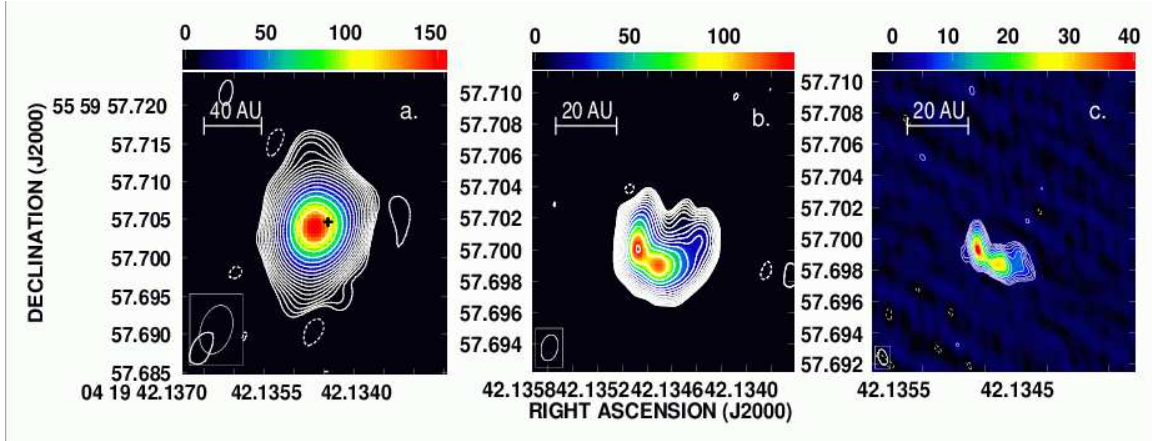


Fig. 3.— VLBA images of CI Cam observed on 5 April 1998. a) 1.7 GHz image: peak flux density 154 mJy/beam (2.4×10^9 K); beam size 6.58×4.28 mas at $34^\circ 5$; rms noise 0.28 mJy/beam; contours at $\pm 2^{n/2} \times 0.45$ mJy/beam, $n = 0, 1, \dots, 14$; conversion to brightness temperature: 16×10^6 K/mJy/beam. b) 5.0 GHz image: peak flux density 131 mJy/beam (3.4×10^9 K); beam size 1.70×1.12 mas at $-14^\circ 3$; rms noise 0.59 mJy/beam; contours at $\pm 2^{n/2} \times 2$ mJy/beam, $n = 0, 1, \dots, 12$; conversion to brightness temperature: 26×10^6 K/mJy/beam. c) 15.3 GHz image: peak flux density 40 mJy/beam (0.35×10^9 K); beam size 1.02×0.58 mas at $18^\circ 8$; rms noise 0.53 mJy/beam; contours at $\pm 2^{n/2} \times 2$, mJy/beam, $n = 0, 1, \dots, 7$; conversion to brightness temperature: 8.7×10^6 K/mJy/beam.

ervation. In addition, the observed 15 GHz flux density would be low by about 50%, in agreement with the actual observations. The only notable distinction which remains is a ~ 14 mJy spur to the northeast of the main emission in the 5 GHz image, which is not seen at 15 GHz. The spectral index of this spur must therefore be somewhat steeper than the $\alpha = -0.38 \pm 0.04$ ($S_\nu \propto \nu^\alpha$) which characterizes the rest of the kidney-shaped structure. For comparison, the overall 5/15 GHz spectral index on this date, as measured with the VLA (Rupen et al., in prep.), is -0.36 .

CI Cam is significantly more extended at 1.7 GHz than at the higher, optically-thin frequencies on 5 April 1998. This is evident in Figure 3, but is shown more clearly in the super-resolved 1.7 GHz image in Figure 5a, where the CLEAN component model is restored with a 3×3 mas beam. Following the same procedure as above, Figure 5b shows the 1.7 GHz model put through the 5 GHz (u, v) -coverage. While the southern, kidney-shaped emission is fairly similar, the northern component is seen only at 1.7 GHz, implying a very different spectral index. Quantitatively, the spectral index of the southern, kidney shaped component between 1.7 and 5 GHz is $\alpha = +0.78 \pm 0.03$, while

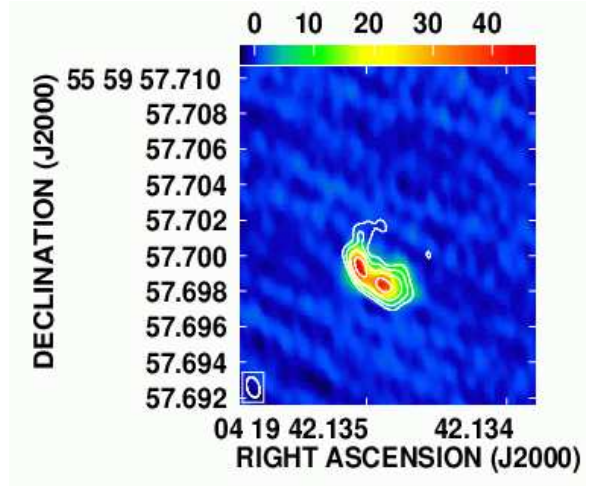


Fig. 4.— Contours: the CLEAN model of the 5 GHz data, put through the (u, v) coverage of the 15 GHz observation (peak flux density 79.0 mJy/beam; beam size 1.18×0.73 mas at $19^\circ 6$; contours at $\pm 2^{n/2} \times 7$ mJy/beam, $n = 0, 2, 4, 6$). Colors: the observed 15 GHz image (peak flux density 47.2 mJy/beam).

that of the northern component must be steeper than -1.0 . This is most readily interpreted as an opacity gradient across the source, with the northern component being much more optically thin.

3.2. June 1998–January 1999

Images from further VLBA observations on 14–21 June, 2 July, and 10 September 1998 are displayed in Figure 6. Since CII Cam does not evolve rapidly the 14 and 21 June data sets were concatenated, significantly improving the resulting image. Figure 7 shows a MERLIN image from 31 January 1999. The crosses in these images indicate the position of the peak of the 1.7 GHz image from 5 April 1998. Several results are obvious from these figures. First, the source does not bear any resemblance to a relativistic jet. Second, CII Cam has significantly expanded, from ~ 12 mas on 5 April 1998, to at least 350 mas in the north-south direction on 31 January 1999, 306 days after outburst. Third, the expansion is roughly symmetric about the center. Fourth, there is significant emission within the source’s outer rim (shell). Finally, the shell’s appearance changes significantly with time, although the position angle of the major axis is constant. In early April, the southern part is the brightest; by June–July the northern portion is brighter, and the structure looks almost like a double ring. In September 1998 the source seems more nearly elliptical, and an area in the south has brightened from 1.9 mJy in June to 2.7 mJy in September, measured at the same position angle on the source and approximately the same area. Unfortunately, the MERLIN resolution is not sufficient to see any morphological details, but the west side is brighter than the east, showing that the source remains asymmetric through at least 31 Jan. 1999. It is also interesting to note that the position angle of the slightly resolved component in the first epoch ($\sim 20^\circ$) is comparable to that of the major axis in these later images, suggesting that this position angle was established within a day of the outburst.

4. Discussion

4.1. Emission Mechanism

The radio emission in CII Cam must be primarily synchrotron, from relativistic particles spiral-

ing around strong magnetic fields. This is based on the high brightness temperatures (up to a few billion Kelvin) seen in the VLBA images, and on the radio spectrum at high frequencies, which follows a steeper power law than allowed for thermal emission. Further, any thermal plasma hot and dense enough to produce the observed radio emission at late times would necessarily produce strong X-ray emission as well, at levels well above what is actually observed (Parmar et al. 2000; Orlandini et al. 2000). Interestingly, the peak brightness temperature in these resolved, optically-thick images is well below the canonical $10^{11} - 10^{12}$ K brightness temperature limit thought to be typical of other synchrotron sources, such as extragalactic jets (e.g., Kellermann & Pauliny-Toth 1969; Readhead 1994) and radio supernovae (e.g., Wieringa, Kulkarni, & Frail 1999). Taking the peak of the 5 April 1998 5 GHz image as an example, assuming energy equipartition between relativistic electrons and the magnetic fields, and taking the ratio of proton to electron energies as $k = 100$ (as in local cosmic rays), the magnetic field is $1.2 d_{5 \text{ kpc}}^{-2/7}$ G, the total energy in relativistic particles and fields is $1.5 \times 10^{41} d_{5 \text{ kpc}}^{17/7}$ erg, and the synchrotron lifetime at 5 GHz is $72 d_{5 \text{ kpc}}^{3/7}$ days. The energy of the electrons producing synchrotron radiation at a frequency ν is then $30 d_{5 \text{ kpc}}^{1/7} (\nu/5 \text{ GHz})^{3/7}$ MeV. These values should be taken as indicative rather than definitive. Nevertheless it is clear that, as usual, the energy in relativistic particles and fields is not an important part of the overall energy budget — the total X-ray emission in the flare for instance was $\sim 9.3 \times 10^{42} d_{5 \text{ kpc}}^2$ erg, while the total integrated luminosity was a factor ~ 600 higher (Frontera et al. 1998). The rapid radio decay further shows that synchrotron losses do not dominate the observed radio light curve, another not-unexpected result.

4.2. Absorption Mechanisms

At early times the radio remnant is optically thick, indicating substantial absorption. The rapid changes in optical depth show that this absorption is associated with the source itself, rather than some unrelated medium. There are two main processes which are relevant here: synchrotron self-absorption (SSA) by the same relativistic electrons which produce the emission, and

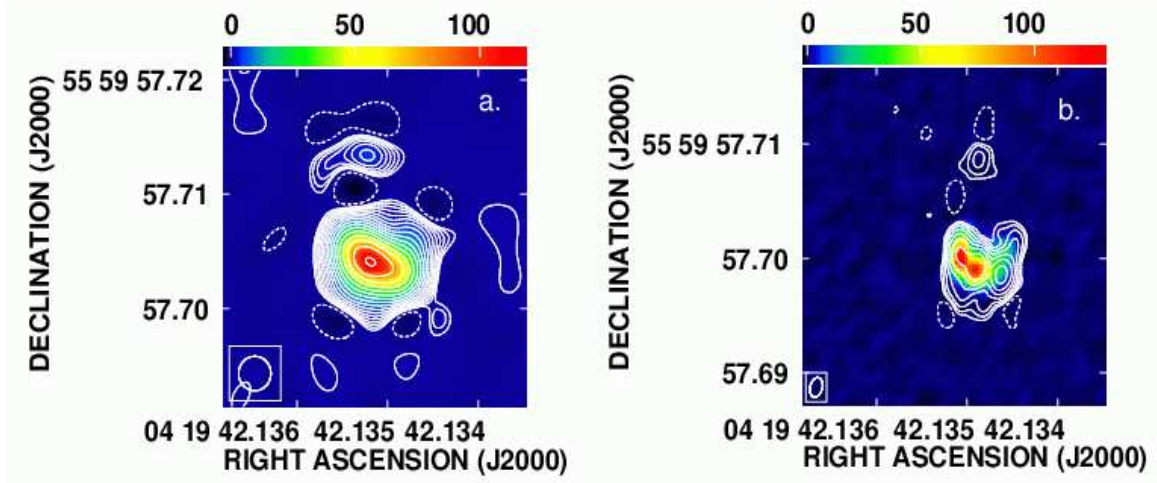


Fig. 5.— a) The 1.7 GHz image, restored with a 3×3 mas beam: peak flux density 1.18 mJy/beam; contours same as in Figure 3a. b) Contours: the CLEAN model of the 1.7 GHz data, put through the (u, v) coverage of the 5 GHz observation (peak flux density 78.0 mJy/beam; beam size 2.03×1.21 mas at $-10^\circ 3'$; contours at $\pm 2^{n/2} \times 0.5$ mJy/beam, $n = 0, 2, \dots, 12$). Colors: the observed 5 GHz image (peak flux density 131.0 mJy/beam).

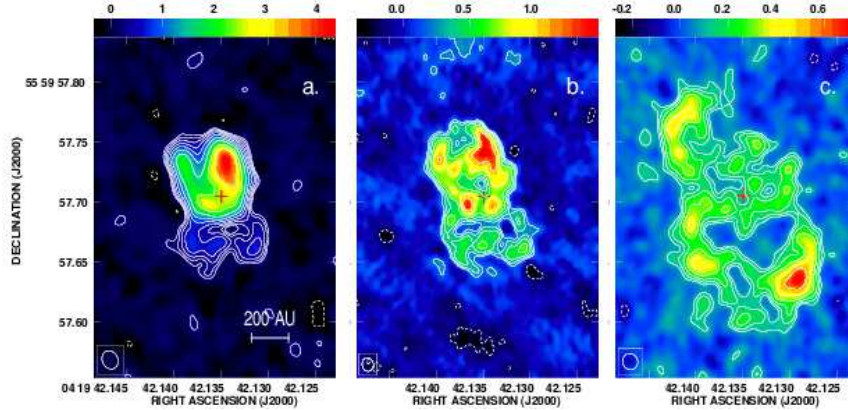


Fig. 6.— 1.7 GHz VLBA images of CI Cam observed months after the X-ray flare. The red crosses mark the position of the peak of the 5 April 1998 1.7 GHz image. a) Combined dataset of 14 and 21 June 1998: peak flux density 4.37 mJy/beam (8.7×10^6 K), beam size 16.13×13.64 mas at $34^\circ 5'$, rms noise 0.075 mJy/beam; contours at $\pm 2^{n/2} \times 0.2$ mJy/beam, $n = 0, 1, \dots, 6$; conversion to brightness temperature: 2.0×10^6 K/mJy/beam. Image made with a Gaussian (u, v) taper of $25 M\lambda$ (at 30%) and natural weighting. b) Image from 2 July 1998: peak flux density 1.45 mJy/beam (5.6×10^6 K), beam size 11.36×10.03 mas at $13^\circ 3'$, rms noise 0.084 mJy/beam; contours at $\pm 2^{n/2} \times 0.2$ mJy/beam, $n = 0, 1, 2, 3, 4$; conversion to brightness temperature: 3.9×10^6 K/mJy/beam. Image made with a Gaussian (u, v) taper of $25 M\lambda$ (at 30%) and natural weighting. c) Image from 10 September 1998: peak flux density 0.734 mJy/beam (1.7×10^6 K), beam size 14.49×13.29 mas at $45^\circ 4'$, rms noise 0.036 mJy/beam; contours at $\pm 2^{n/2} \times 0.1$ mJy/beam, $n = 0, 1, \dots, 5$; conversion to brightness temperature: 2.3×10^6 K/mJy/beam. Image made with a Gaussian (u, v) taper of $15 M\lambda$ (at 30%) and natural weighting.

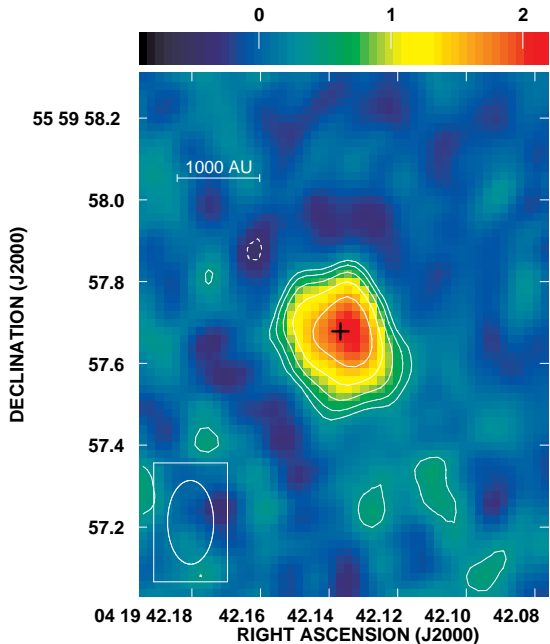


Fig. 7.— 4.99 GHz MERLIN image of CI Cam on 31 January 1999. Peak flux density 2.159 mJy/beam (4.6×10^3 K), beam size 204.69×112.70 mas at $0^\circ 3$, rms noise 0.15 mJy/beam; contours at $\pm 2^{n/2} \times 0.4$ mJy/beam, $n = 0, 1, 2, 3, 4$; conversion to brightness temperature: 2.1×10^3 K/mJy/beam. Image made with a Gaussian (u, v) taper of $2M\lambda$ (at 30%) and natural weighting. The black cross, as in Figures 2, 3a and 6, marks the position of the peak of the 5 April 1998 1.7 GHz image. The alignment should be good to a few milliarcseconds.

free-free absorption by dense ionized gas along the line-of-sight. The equipartition magnetic field derived above would produce an SSA cutoff frequency of $\sim 3.0 d_{5 \text{ kpc}}^{2/35}$ GHz; below this frequency the emission should be optically thick, with a characteristic $\nu^{2.5}$ spectrum. This is consistent with the observed 1.7 and 5 GHz flux densities on 5 April 1998, which imply a turnover frequency around 2.4 GHz. The northern component, seen only at 1.7 GHz, could easily be optically thin on the same date, since its much lower flux density yields a predicted SSA turnover below 1 GHz. At the same time the emission from the main, southern region must truly be as smooth as it appears in these images: any significant clumping would

lead to brightness temperatures above $\sim 10^{10}$ K, corresponding to SSA turnover frequencies above 5 GHz.

CI Cam is also known to have a dense stellar wind, which could lead to substantial free-free absorption. To produce unit opacity at 3 GHz requires an emission measure ($\int n_e^2 dl$) of $\sim 3.2 \times 10^7 (T_e/10^4 \text{ K})^{1.35} \text{ pc cm}^{-6}$, where T_e is the electron temperature, n_e is the electron number density, and l is the line-of-sight path length. Taking an $n_e \propto r^{-2}$ wind, assuming cosmic abundances, and taking the inner radius of the absorbing material to be 10 AU (corresponding roughly to the size of the 5 April 1998 emission region), this gives a density at 10 AU of $\sim 3 \times 10^{-18} (T_e/10^4 \text{ K})^{0.675} \text{ g cm}^{-3}$. For comparison the modeled density for the wind in the sgB[e] star HD 87643 at 10 stellar radii is $10^{-16} - 10^{-15} \text{ g cm}^{-3}$ and $10^{-12} \text{ g cm}^{-3}$ for the hot diffuse and cold dense winds, respectively (Oudmaijer et al. 1998). Free-free absorption could thus be quite significant, depending on the relative orientation of the winds and the radio-emitting region, and on the temperature and ionization of the winds. In sum, synchrotron self-absorption must be important in the early radio remnant, but free-free absorption may also play a role. A detailed analysis of the multi-frequency radio light curve may break this degeneracy.

Even without any absorption, the radio remnant shows significant spectral variations: the northern component seen at 1.7 GHz on 5 April 1998 must for instance have an intrinsic emission spectrum (ν^{-1} or steeper) which is much steeper than the rest of the source ($\nu^{-0.4}$). Such extreme variations have not been seen in other shell-like sources, such as radio supernovae (Bietenholz et al., priv. comm.) and supernova remnants (e.g., Wright et al. 1999; Delaney et al. 2002). The explanation may lie in the very complex environment around CI Cam, which could plausibly lead to very different densities and magnetic fields in different parts of the circumstellar medium.

4.3. Morphology

The basic appearance of CI Cam's radio remnant (edge-brightened, clumpy, shell-like) strongly suggests a shock plowing into a dense circumstellar medium. The radio emission from all other X-ray transients has been either unresolved, or consis-

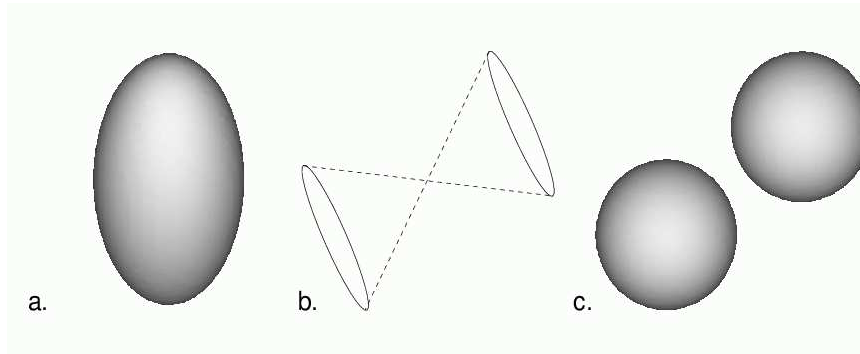


Fig. 8.— Three possible models for the three-dimensional structure of IC Cam. (a) An ellipsoid, where patches of the surface are lit up; (b) the ends of a two-sided cone (note that these must both move out and widen with time); (c) two spheres. Both the cone and the spheres, for some inclinations, could produce the appearance of overlapping circles in later images (Figure 6). The ellipsoid would require some patchiness in the surface, analogous to the brightness variations seen around the rim. The observer is to the right.

tent with a highly collimated one- or two-sided jet; but there is certainly no sign of a jet in these images, and the continued brightness of the remnant despite substantial expansion requires on-going particle acceleration. The relative brightness of various features changes substantially from epoch to epoch, with some parts of the remnant even brightening despite the overall decay; but the overall shape remains fairly constant (see below). The basic implication is that we are seeing the evolving results of an explosion inside a dense, clumpy environment, much like a radio supernova. The changing appearance then corresponds to changes in the local shock strength, the particle acceleration efficiency, or the synchrotron emissivity; these in turn are presumably functions of the local particle density and magnetic field strength and orientation.

Even in our last image, the remnant shock is only ~ 350 mas ($1750 d_{5kpc}$ AU) across, and is thus still running into material dominated by IC Cam’s stellar wind. The highly asymmetric and clumpy radio morphology probably implies a similarly anisotropic and inhomogeneous circumstellar medium (CSM), which seems more likely than a severely asymmetric explosion or magnetic field, and is consistent with other indications of a highly anisotropic wind (Robinson, Ivans, & Welsh 2002; Hynes et al. 2002). The idea of a dense surrounding medium is also supported by X-ray observations of IC Cam in quiescence, which show

strong and highly variable absorption (Parmar et al. 2000; Boirin et al. 2002), and by IC Cam’s strong infrared excess (Dong & Hu 1991; Allen & Swings 1976). In this picture the changing appearance of the remnant reveals the variations in the density of the CSM. The initial bright kidney shaped structure to the south (Figure 3b and c) was presumably due to a particularly dense clump on that side, which has been over-run by the time of the June-July images (Figure 6a and b); while the initially fainter emission to the north indicates a lack of dense material on that side. Robinson, Ivans, & Welsh (2002) and Hynes et al. (2002) suggest that the outflow from IC Cam consists of a slow (~ 30 km/s), dense equatorial wind, and a fast (~ 1000 km/s), less dense polar wind. The shock seen in the radio emission between 2 July 1998 and 10 September 1998 then traces out 250/8200 years of stellar mass loss, during which time the density of the stellar wind changed from most dense in the north-west to most dense in the south-west; while the similarity between the June and July maps shows that the wind did not vary dramatically on shorter timescales (75/2500 years). Significant stellar wind variations are not unprecedented. Optical images of ICR+10216, for instance, reveal discrete incomplete rings of dust, which imply that the mass loss rate of the star changes on a hundred year timescale, and is not spherically symmetric (Mauron & Huggins 1999).

Despite these changes in brightness across the

source, the overall structure is quite similar from epoch to epoch: that is, the brightest regions move outward at the same rate as the dim ones. This suggests that the radio synchrotron emission simply serves to ‘light up’ the edges of the shock, while remaining energetically unimportant. By itself this is not so surprising, as the luminosities are so low, but this further implies that the particle acceleration, and whatever causes it to vary around the source, is also not dynamically important. This is a common result for shocks. The radio remnant of SN 1993J, for instance, exhibits changing 3:1 brightness asymmetries around a shell which decelerates but remains highly circular (Bietenholz, Bartel, & Rupen 2001; Bartel et al. 2002; Bietenholz, Bartel, & Rupen 2003) and the supernova remnant SN 1006 has huge brightness asymmetries around a similarly circular rim (Roger et al. 1988).

4.3.1. *CICam in three dimensions*

As with most astronomical imaging, these data show a two-dimensional projection of a three-dimensional object. The radio remnant is clearly elongated, so the intrinsic structure must also be asymmetric, either due to an off-center explosion, or to an asymmetry in the surrounding medium. One puzzle is that the source retains a similar appearance while slowing down considerably (see below). Several possible geometries, which could explain the overall appearance, are shown in Figure 8.

An ellipsoid could explain the outer shape of the remnant, with the brighter regions in the middle caused by some minor asymmetry in the particle acceleration/emission process along the line-of-sight to the center. However, it is difficult to retain the axis ratio of such an ellipsoid over time. Any three-dimensional structure confined by denser material around the ‘waist’ would be expected to become more and more elongated over time, as the material in the waist should decelerate more rapidly than that at the poles. Edge-brightened cone rims could result from a shock lighting the densest regions of a dense wind, as in some planetary nebulae, while a pair of spherical bubbles might arise in an explosion in a highly asymmetric environment. Figure 9 shows a tilted circular ring and a two-sided tilted cone that were fit to the data; note that the rims of the cone

both move outward and expand with time. In both cases the expansion rate is $\sim t^{0.8}$, as discussed in the next section. The angle between the normal to the tilted ring and the line-of-sight is $53^\circ \pm 5^\circ$, while the angle between the cone axis and the line-of-sight is $23^\circ \pm 3^\circ$. These fits are illustrative rather than unique. The two-sided cone seems to fit marginally better as it takes into account the waist of the nebula. The results for a pair of spherical bubbles would be similar to those for the two-sided cone.

4.4. Expansion

The expansion rate of CICam can be fit regardless of the model used to explain the morphology, assuming that the source remains self-similar throughout. Figure 10 shows the results of fitting an ellipse to each image; the axis ratio is constant at 1.9:1, and this plot shows the expansion of the major axis as a function of time. The shock is clearly decelerating, presumably because of material swept up from the wind as the shock expands. The average radial expansion rate of the major axis between an assumed explosion date of 31.64 March 1998 (corresponding to the first X-ray detection) and 5 April 1998 is $\sim 1.4 \text{ mas/day} = 11,000 d_5 \text{ kpc km/s}$. This means during the 5 April 1998 observations the source expanded by $\sim 0.5 \text{ mas}$. Since the beam is bigger than this for the 1.7 and 5 GHz images this would have no effect. However $\sim 0.5 \text{ mas}$ is comparable to the 15 GHz beam and therefore the motion may have smeared the image slightly in the direction of motion. This is probably insignificant though, since the structures in this image are $> 3 \text{ mas}$. Between the first X-ray detection and the MERLIN image (January 1999) the *average* expansion is $\sim 0.6 \text{ mas/day} = 5,000 d_5 \text{ kpc km/s}$. A power-law gives a reasonable fit to the expansion data: $\Theta = (4.2 \pm 0.9)(t - 50904.09 \pm 0.64)^{0.77 \pm 0.04}$, where Θ is the major axis in mas, t is the Modified Julian Date (MJD), and the error bars are 1σ assuming normally-distributed errors and forcing $\chi^2_\nu \sim 1$. The implied radial velocity is $v = 14,000(t - 50904.09)^{-0.23} \text{ km/s}$. While only poorly determined, the explosion date is consistent with the beginning of the X-ray flare (on MJD 50903.64), and the fit is consistent with CICam being marginally resolved in the first epoch ($\Theta = 3.6 \text{ mas}$). This expansion rate ($t^{0.77}$) is much faster

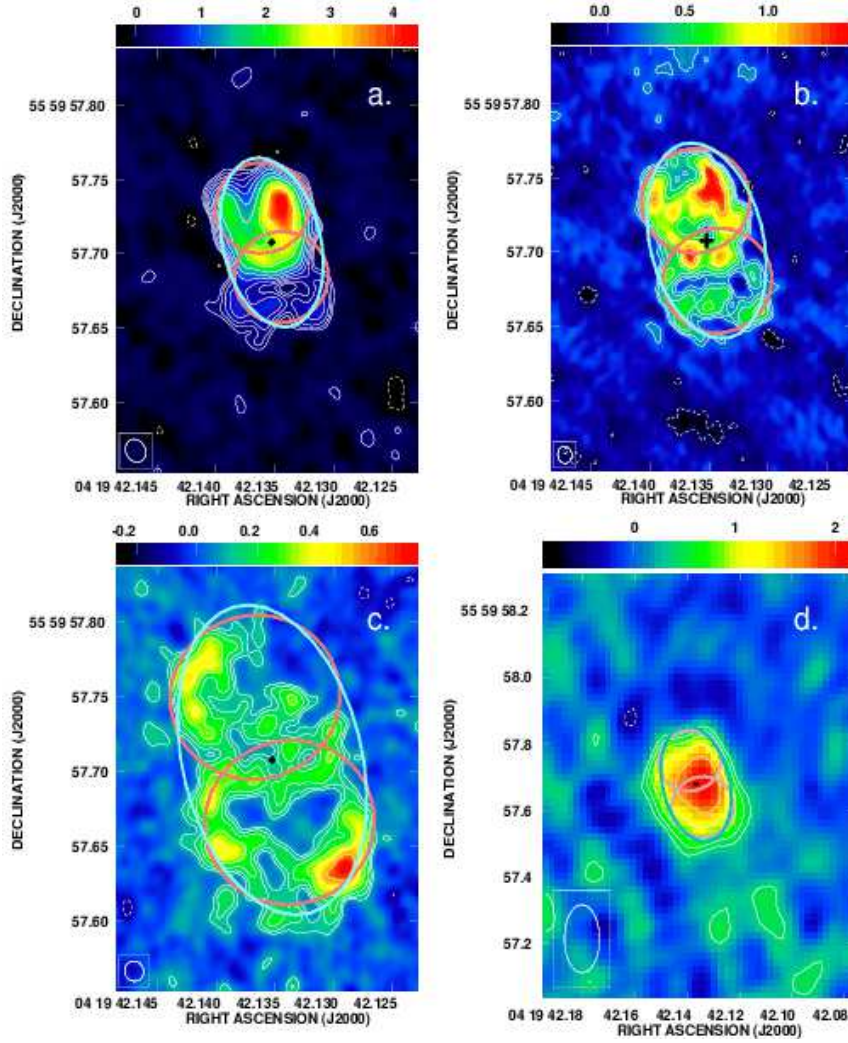


Fig. 9.— Images from (a) June 1998, (b) July 1998, (c) September 1998, and (d) January 1999, overlaid by models of a tilted ring (cyan) and two-sided cone (orange). The contour levels are the same as in Figures 6 and 7. The parameters of the tilted ring model are: radius $\propto t^{0.8}$, angle between normal and line-of-sight $53^\circ \pm 5^\circ$, and position angle 15° east of north. The parameters of the tilted two-sided cone model are: radius $\propto t^{0.8}$, angle between cone axis and line-of-sight $23^\circ \pm 3^\circ$, cone opening angle 31° , and position angle 7° east of north.

in than the classic Sedov phase seen in supernovae remnants ($t^{0.4}$), but is consistent with young supernovae (e.g., for SN 1993J $R \sim t^{0.92-0.78}$ [Bartel et al. 2002]).

Given the density of CICam’s circumstellar medium, the initial impulsive energy injection must have been quite strong to produce such a fast shock. One quantitative estimate comes from the changing X-ray absorption column seen at

early times (Belloni et al. 1999). This implies column densities N of a few $\times 10^{22} \text{ cm}^{-2}$ which decline by more than a factor of ten over the first two days. It seems reasonable to associate this decline with the forcible removal of material by the shock seen in the radio images. By the time the X-ray absorption has decayed away on 2 April (Belloni et al. 1999) the shock was $\sim 5.4 \text{ mas} = 4 \times 10^{14} d_{5 \text{ kpc}} \text{ cm}$ across, according

to the above fit. The total number of atoms swept up was $\sim Nr^2 \sim 8 \times 10^{51} d_{5\text{ kpc}}^2$, giving an average density of $\sim N/r \sim 10^8 d_{5\text{ kpc}}^{-1} \text{ cm}^{-3}$, or $\sim 3 \times 10^{-16} d_{5\text{ kpc}}^{-1} \text{ g/cm}^3$, assuming an average mass per atom of 1.4 times the mass of a proton. These values are well within the range implied by spectroscopy during the outburst ($< 10^5$ to $> 10^{10} \text{ cm}^{-3}$: Clark, Steele, Fender, & Coe 1999; Orlandini et al. 2000; Robinson, Ivans, & Welsh 2002; Hynes et al. 2002; Miroshnichenko, Klochkova, Bjorkman, & Panchuk 2002), and not inconsistent with models of the winds in sgB[e] stars (e.g., Oudmaijer et al. 1998). The total mass swept up by the shock was then of order $2 \times 10^{28} d_{5\text{ kpc}}^2 \text{ g}$, giving a corresponding kinetic energy (at $13,500 d_{5\text{ kpc}} \text{ km/s}$) of $\sim 2 \times 10^{46} d_{5\text{ kpc}}^4 \text{ erg}$. This number is very uncertain, given all the underlying assumptions. Even so it is clear that the kinetic energy in the shock could easily match or exceed the integrated luminosity of the outburst across all observed wavelengths ($\sim 6 \times 10^{45} d_{5\text{ kpc}}^2$, Frontera et al. 1998).

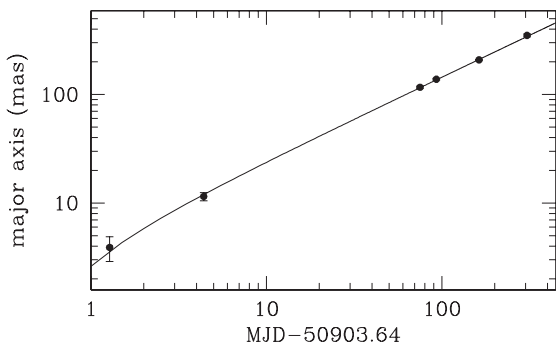


Fig. 10.— The expansion of the major axis of CI Cam versus time, where time is in days after the first X-ray detection on MJD 50903.64. The major axis is estimated by fitting ellipses to the images; the errors are taken from the quality of that fit, scaled down by a factor ~ 6 to give $\chi^2 \sim 1$ for the power-law model. The five early points are taken from the 1.7 GHz VLBA images shown in Figures 2, 3a, and 6. The latest point is based on the 5 GHz MERLIN observation shown in Figure 7. The line is a least squares fit to the data, $\Theta = (4.2 \pm 0.9)(t - 50904.09 \pm 0.64)^{0.77 \pm 0.04}$, with Θ in milliarcseconds and t in days.

The continued slow deceleration of the shock

can be used to place constraints on the distribution of the circumstellar material via the shock jump conditions, in a manner analogous to (Chevalier 1982)’s treatment of the expansion of radio supernovae. Actually what is derived is a relationship between the density structure of the outer regions of the ejecta, and that of the CSM. Here the ‘ejecta’ should be thought of as the material swept up by the time of the first observation; while this is the stellar envelope in the case of a supernova, for CI Cam it is probably more appropriate to think of dense material surrounding (accreting onto?) the compact object. The shock between ejecta with outer density profile $\rho_{ej} \propto R^{-n}$ and a CSM with density profile $\rho_{CS} \propto R^{-b}$ will expand at a rate $R \propto t^m$, with $m = (n - 3)/(n - b)$. The observed $m = 0.77$ is well within the range observed for radio supernovae (e.g., Bartel et al. 2002), and suggests $n \sim 6.3$ for an R^{-2} wind profile. More generally one can argue that the observed deceleration implies that the shock has swept up a significant amount of mass, compared to that of the original ejecta. The factor two drop in velocity at late times implies a factor two to four increase in the mass over the same interval, assuming momentum or energy conservation, respectively.

4.4.1. Optical Doppler shifts

Data taken before the April 1998 outburst showed a stable spectrum dominated by symmetric, single-peaked hydrogen Balmer lines, with wings extending to $\pm 250 \text{ km/s}$ (Hynes et al. 2002). During the outburst both H I and He I lines became much broader and asymmetric, with line wings extending up to 2500 km/s in H α and He I on 3 April 1998, and perhaps out to $\sim 5000 \text{ km/s}$ in the blue wing of H α (Hynes et al. 2002). Robinson, Ivans, & Welsh (2002) also see $\sim 2500 \text{ km/s}$ line wings in H and He on 9 April 1998. While these broad wings faded fairly quickly (Hynes et al. 2002), an ultraviolet spectrum taken two years after the outburst showed P Cygni profiles with absorption wings extending to $\sim -1000 \text{ km/s}$ (Robinson, Ivans, & Welsh 2002). It seems natural to associate these broad lines with the outflow imaged at radio wavelengths. The proper motions from our images correspond to a radial expansion of the major axis at $\sim 14,000 d_{5\text{ kpc}} (t - 50904.09)^{-0.23} \text{ km/s}$. The

shock velocity was thus $\sim 11,000d_{5kpc}$ km/s on 3 April, and $\sim 8,600d_{5kpc}$ km/s on 9 April 1998; extrapolating to two years after the outburst gives an expected velocity of $\sim 3,100d_{5kpc}$ km/s. The corresponding expansion velocities of the minor axis of the fitted ellipse are 60% of these values.

There are many uncertainties in comparing the radio proper motions with the optical Doppler shifts. First, the source is clearly asymmetric, both from the radio images and from the optical line shapes at early times, which makes the comparison of radial with transverse velocities somewhat suspect. Second, while the radio emission traces the motions of the outer ejecta, the optical lines could be sampling very different regions, with different kinematics. This is often seen in supernovae (e.g., Bietenholz, Bartel, & Rupen 2001), and is clearly the case for CI Cam at later times, when no substantial line wings are seen. Given the difficulties the rough agreement between optical and radio velocities is remarkable, and suggests that the distance to the source is within a factor two of the nominal 5 kpc we have adopted.

4.5. CI Cam as a stellar outflow

There are some similarities between the radio morphology of CI Cam and the radio outflows/nebulae observed in other stars (e.g., AG Pegasi [Kenny, Taylor, & Seaquist 1991] and HM Sagittiae [Eyres et al. 1995; Hack & Paresce, F. 1993; Eyres et al. 2000]), as well as optical outflows around planetary nebulae (PNe) (Balick & Frank 2002) and the high mass star Eta Carinae (Morse et al. 1998). The hourglass and double ring structures seen in many PNe is thought to be caused by the density structure of the circumstellar material into which the ejected material expands (Balick & Frank 2002); this is very similar to our picture of CI Cam's remnant. However, the optical emission from PNe has a very different physical origin from the radio synchrotron seen in CI Cam, as does the radio emission from most stellar outflows (thermal free-free radiation). The expansion rate in CI Cam is also much larger than the 10 km/s to 1000 km/s seen in other stars (e.g., Eyres et al. 1995; Kenny, Taylor, & Seaquist 1991; Palen et al. 2002).

The overall structure of the CI Cam radio remnant (a clumpy shell), its initial expansion speed ($\sim 10,000 d_{5kpc}$ km/s), and its gradual decelera-

tion are all very similar to what is seen in radio supernovae (e.g., SN 1993J: Bartel et al. 1994; Marcaide et al. 1995; Bartel et al. 2002). There are however two basic differences. First, the radio shell in CI Cam is decidedly asymmetric, while the few resolved radio supernovae are basically circular. Supernova remnants on the other hand are often asymmetric, which (as in CI Cam) is most readily interpreted as the result of a shock running into a severely anisotropic medium. Second, while radio supernovae – and indeed, virtually all resolved, optically-thin radio sources – have rather steep radio spectra ($\alpha \sim -0.7$ to -1.0), CI Cam retains a much flatter $\alpha \sim -0.4$ for many months. Since the optically-thin spectral index is a direct consequence of the energy distribution of the relativistic electrons, this requires a very unusual (but also quite stable) particle acceleration process.

4.6. CI Cam as an X-ray transient

While radio emission is often associated with X-ray transients and binaries (e.g., Hjellming & Han 1995; Fender & Kuulkers 2001), CI Cam is unique in showing a slowly-expanding, two-dimensional remnant. In all other cases, any resolved radio emission is dominated either by separable ejecta, or by a collimated jet, often moving at relativistic speeds (e.g., Mirabel & Rodriguez 1994; Hjellming & Rupen 1995; Fomalont, Geldzahler, & Bradshaw 2001; Mioduszewski et al. 2001; Blundell et al. 2001; Gallo et al. 2004). This has led to the wide-spread assumption that radio emission from X-ray binaries always indicates the presence of a relativistic jet, and many models now take radio emission as the best unambiguous tracer of jet emission (e.g., Fender 2003). CI Cam throws this entire paradigm into doubt. Does this have wider implications for X-ray binaries in general? or is CI Cam truly unique?

4.6.1. CI Cam as a collapsar?

One possibility is that CI Cam did indeed produce a fast jet, but this jet was quickly smothered by the dense surrounding material. In this model the energy in the jet was converted into a less directed outflow, which we see as a shock moving out into the CSM. This is similar to the failed-jet model for supernova explosions in collapsars (e.g., MacFadyen, Woosley, & Heger 2001). Quantitatively, one expects a relativistic jet to slow catas-

trophically when it has swept up an equivalent rest mass energy (e.g., Rhoads 1997; Sari, Piran, & Halpern 1999):

$$E_{jet} = \frac{4}{3}\pi c^2 \langle \rho \rangle r_{stop}^3$$

where E_{jet} is the energy in the jet, and $\langle \rho \rangle$ is the average density within the radius r_{stop} at which the jet slows catastrophically. This equation is appropriate to a jet which is stopped quickly enough that lateral expansion can rapidly isotropize the energy. For CI Cam, we know that the remnant is far from jet-like by a radius of 6 mas ($30d_5$ AU), and according to the arguments in §4.4 the energy in the shock (in this model derived entirely from the original jets) is of order $\sim 2 \times 10^{46} d_5^4$ erg. This gives a lower limit to the mean density required to stop the jets of $\langle \rho \rangle \gtrsim 10^{-19} d_5$ g/cm³, well within the plausible range for the wind of a sgB[e] star. It is interesting to note that simulations of “stalled” jets in the context of γ -ray bursts predict morphologies very similar to what we see in CI Cam (see particularly the 36°-inclination images in Figures 8 and 9 of Ayal & Piran 2001).

The question arises as to why other jets are not similarly smothered. Most other X-ray transients live in relatively pristine environments, where the jet might more easily escape. In binaries with substantial circumstellar material the accretion tends to be more continuous (e.g., Cyg X–3 and SS 433), and the resulting jets are also ‘on’ more often, and are thus perhaps capable of sweeping away the CSM. This fits in with Hynes et al. (2002)’s picture of the CI Cam outburst, in which a compact object in a highly eccentric long-period (> 100 years) orbit moves through the dense equatorial wind of its companion star; the brief period of super-critical accretion, when the compact object is close to the companion, leads to the X-ray flare and the expanding radio shock front. A long-period orbit is required to explain the lack of previous known flares, which would have been obvious in the optical to historical astronomers.

4.6.2. Shock signatures and implications for other X-ray transients

Given that CI Cam’s radio remnant is clearly dominated by a shock, it is natural to ask whether the emission at other wavelengths could also be associated with that shock, rather than with the

accretion disk. Extrapolation of the radio synchrotron spectrum to other wavelengths shows that the expected synchrotron emission is far below that observed during the outburst (Belloni et al. 1999; Hynes et al. 2002). Similarly the thermal emission produced by the shock is likely to be quite modest, for three reasons. First, the shock has not had enough time to become radiative, for any reasonable densities. Second, the characteristic temperature of the forward shock (~ 300 keV for a 10,000 km/s shock) (a) lies outside the passband of most available instruments, and (b) puts the shocked gas in a regime where cooling is quite slow. Third, while the reverse shock should be slower and hence lead to lower and more easily observable temperatures, the resulting fluxes are likely to be very low; scaling from the radio/X-ray ratios in observed supernovae for instance (e.g., Pooley et al. 2002) the expected emission is orders of magnitude below the observed flux during the outburst. The observed soft X-rays, in this as in other X-ray transients, probably arise in and around the accretion disk rather than in the shock. Thus the only obvious signatures of the shock outside the radio remnant are the optical and UV spectral lines. Some of these are Doppler broadened by a thousand or more km/s; others evolve very rapidly, requiring very high densities, as might result from a shock (Hynes et al. 2002). Recent spectra (2001-2002) still show many spectral lines at very different strengths than their very stable pre-outburst levels (Hynes et al. 2002; Miroshnichenko, Klochkova, Bjorkman, & Panchuk 2002), which suggests some continued disturbance around the binary. None of these is really a ‘smoking gun,’ indicating that, for an unresolved X-ray transient, a shock and a freely expanding jet may not be distinguishable.

It does not however seem likely that the radio emission from many other unresolved X-ray binaries can be fully explained by shocks similar to that seen here. CI Cam’s radio light curve is unusual in showing a single outburst followed by a smooth, steep-spectrum ($S_\nu \propto \nu^{-0.4}$) decay. Outbursts from other sources often lead to multiple radio events, suggesting strong on-going activity more readily associated with the central source than with a single expanding shock wave. There could be a series of shocks of course, but that requires re-furbishing the surrounding medium on rather fast timescales (days to weeks). On the

other hand, this single shock evacuating the surrounding medium may explain why there was only one explosive event, i.e., the shock got rid of any additional material that could have been accreted by the compact object, and the compact object moved away from the high density region before the stellar wind could replenish the material. The quasi-steady radio emission seen in the low/hard state is also very different from CI Cam's optically-thin remnant, and requires a very small and continuously replenished radio source. Given these indications of very different power sources, it is quite surprising that CI Cam lies nicely on the loose X-ray/radio correlation found for X-ray binaries (Fender & Kuulkers 2001; Gallo, Fender, & Pooley 2003), with a scatter typical of other X-ray transients. It is far from obvious why direct synchrotron emission from jets should have the same efficiency as particle acceleration in an expanding shock.

5. Conclusions

We have presented evidence that the radio remnant of CI Cam's 1998 outburst takes the form of a clumpy, decelerating shell, strongly suggesting an expanding shock front, rather than the relativistic jets seen in many other X-ray transients. We suggest that the reason for this distinction lies in CI Cam's very dense stellar wind, which could easily convert even quite energetic jets to a quasi-spherical outflow. The very broad spectral lines seen in optical emission early on, and in the ultraviolet several months later, seem to be the only other unambiguous signatures of this outflow. Associating the radio outflow with those Doppler shifts suggests that the adopted distance of 5 kpc is probably good to a factor of two. Assuming the changing X-ray absorption at early times is due to circumstellar material removed from the line-of-sight by the radio shock, we estimate the shock energy as $\sim 2 \times 10^{46} d_{5 \text{ kpc}}^4$ erg, comparable to the total integrated luminosity of the outburst. If the smothered jet model is correct, this represents one of the very few measurements of a jet's total kinetic energy. The relativistic jets seen in other X-ray binaries and transients must either be much more powerful, or be expanding through much less dense material. The radio light curves of most unresolved sources suggest continued emission from a small region, so it also seems unlikely

that extended shocks dominate the radio emission for these sources. CI Cam seems to be related to other X-ray transients, as collapsar supernovae are related to γ -ray bursts.

This paper would not have existed without Robert Hjellming, who provided the drive to observe this source with the VLBA even before we knew it was a strong radio source. He also edited the first 40 days of the GBI data. We are further indebted to Vivek Dhawan, Kristy Dyer, Dale Frail, and Rob Hynes for useful discussions. The VLA and the VLBA are facilities of NRAO which is operated by Associated Universities, Inc. under cooperative agreement with the National Science Foundation. The GBI is a facility of the National Science Foundation operated by the National Radio Astronomy Observatory (NRAO) in support of NASA High Energy Astrophysics programs. A.J.M. acknowledges support from the European Commission's TMR/LSF Programme (Contract No. ERB-FMGE-CT95-0012). Basic research in radio astronomy at the Naval Research Laboratory is funded by the Office of Naval Research. This research has made use of the SIMBAD database, operated at CDS, Strasbourg, France, and NASA's Astrophysics Data System.

REFERENCES

- Allen, D. A. & Swings, J. P. 1976, *A&A*, 47, 293
- Altenhoff, W. J., Braes, L. L. E., Olon, F. M., & Wendker, H. J. 1976, *A&A*, 46, 11
- Ayal, S. & Piran, T. 2001, *ApJ*, 555, 23
- Balick, B. & Frank, A. 2002, *ARA&A*, 40, 439
- Bartel, N. et al. 2002, *ApJ*, 581, 404
- Bartel, N. et al. 1994, *Nature*, 368, 610
- Bietenholz, M.F., Bartel, N., & Rupen, M.P. 2001, *ApJ*, 557, 770
- Bietenholz, M.F., Bartel, N., & Rupen, M.P. 2003, *ApJ*, 597, 374
- Belloni, T. et al. 1999, *ApJ*, 527, 345
- Blundell, K. M., Mioduszewski, A. J., Muxlow, T. W. B., Podsiadlowski, P., & Rupen, M. P. 2001, *ApJ*, 562, L79

- Boirin, L., Parmar, A. N., Oosterbroek, T., Lumb, D., Orlandini, M., & Schartel, N. 2002, *A&A*, 394, 205
- Chevalier, R.A. 1982, *ApJ*, 259, 302
- Clark, J. S., Steele, I. A., Fender, R. P., & Coe, M. J. 1999, *A&A*, 348, 888
- Clark, J. S. et al. 2000, *A&A*, 356, 50
- Chkhikvadze 1970, *Astrofizika* 6, 65
- Cornwell, T.J., Braun, R., & Briggs, D.S. 1999, in *Synthesis Imaging in Radio Astronomy II*, eds. G.B. Taylor, C.L. Carilli, & R.A. Perley (San Francisco: Astronomical Society of the Pacific), 151
- Delaney, T., Koralesky, B., Rudnick, L., & Dickel, J.R. 2002, *ApJ*, 580, 914
- Dong, Y. & Hu, J. 1991, *Acta Astrophysica Sinica*, 11, 172
- Downes, R.A. 1984, *PASP*, 96, 807
- Eyres, S.P.S., Bode, M.F., O'Brien, T.J., Watson, S.K., & Davis, R.J. 2000, *MNRAS*, 318, 1086
- Eyres, S.P.S., Kenny, H.T., Cohen, R.J., Lloyd, H.M., Dougherty, S.M., Davis, R.J., & Bode, M.F., 1995, *MNRAS*, 274, 317
- Fender, R.P. & Kuulkers, E. 2001, *MNRAS*, 324, 923
- Fender, R. 2003, in *Compact Stellar X-ray Sources*, eds. W.H.G. Lewin & M. van der Klis, in press (also astro-ph/0303339)
- Fomalont, E.B., Geldzahler, B.J., & Bradshaw, C.F. 2001, *ApJ*, 558, 283
- Frontera, F. et al. 1998, *A&A*, 339, L69
- Gallo, E., Corbel, S., Fender, R.P., Maccarone, T.J., & Tzioumis, A.K. 2004, *MNRAS*, 347, L52
- Gallo, E., Fender, R.P., & Pooley, G.G. 2003, *MNRAS*, 344, 60
- Greisen, E.W. 2003, in *Information Handling in Astronomy – Historical Vistas*, ed. A. Heck (Dordrecht: Kluwer Academic Publishers), 109
- Hack, W.J., Paresce, F., 1993, *PASP*, 105, 1273
- Harmon, B. A., Fishman, G. J., & Paciesas, W. S. 1998, *IAU Circ.* 6874 1
- Harmon, B. A., et al., 2004, *ApJS*, in press
- Hjellming, R.M. & Han, X. 1995, in *X-ray Binaries*, eds. W.H.G. Lewin, J. van Paradijs, & E.P.J. van den Heuvel (New York: Cambridge University Press), 308
- Hjellming, R.M. & Mioduszewski, A.J. 1998, *IAU Circ.* 6862
- Hjellming, R.M. & Mioduszewski, A.J. 1998, *IAU Circ.* 6872
- Hjellming, R.M. & Rupen, M.P. 1995, *Nature*, 375, 464
- Hynes, R.I. et al. 2002, *A&A*, 392, 991
- Kellermann, K.I. & Pauliny-Toth, I.I.K. 1969, *ApJ*, 155, L71
- Kenny, H.T., Taylor, A.R., & Seaquist, E.R., 1991, *ApJ*, 366, 549
- MacFadyen, A. I., Woosley, S. E., & Heger, A. 2001, *ApJ*, 550, 410
- Marcaide, J. M. et al. 1995, *Nature*, 373, 44
- Mauron, N. & Huggins, P. J. 1999, *A&A*, 349, 203
- Mioduszewski, A. J., Rupen, M. P., Hjellming, R. M., Pooley, G. G., & Waltman, E. B. 2001, *ApJ*, 553, 766
- Mirabel, I. F. & Rodriguez, L. F. 1994, *Nature*, 371, 46
- Miroshnichenko, A. S., Klochkova, V. G., Bjorkman, K. S., & Panchuk, V. E. 2002, *A&A*, 390, 627
- Morse, J. A., Davidson, K., Bally, J., Ebbets, D., Balick, B., & Frank, A. 1998, *AJ*, 116, 2443
- Orlandini, M. et al. 2000, *A&A*, 356, 163
- Oudmaijer, R. D., Proga, D., Drew, J. E., & de Winter, D. 1998, *MNRAS*, 300, 170
- Palen, S., Balick, B., Hajian, A. R., Terzian, Y., Bond, H. E., & Panagia, N. 2002, *AJ*, 123, 2666

- Parmar, A. N., Belloni, T., Orlandini, M., Dal Fiume, D., Orr, A., & Masetti, N. 2000, *A&A*, 360, L31
- Pooley, D. et al. 2002, *ApJ*, 572, 932
- Readhead, A.C.S. 1994, *ApJ*, 426, 51
- Revnivtsev, M.G., Emel'Yanov, A.N., & Borozdin, K.N. 1999, *Astron. Lett.*, 25, 294
- Rhoads, J.E. 1997, *ApJ*, 487, L1
- Robinson, E.L., Ivans, I.I., & Welsh, W.F. 2002, *ApJ*, 565, 1169
- Roger, R.S., Milne, D.K., Kestevan, M.J., Wellington, K.J., & Haynes, R.F. 1988, *ApJ*, 332, 940
- Rupen, M.P., Mioduszewski, A.J., & Hjellming, R.M. 2003, *Proceedings of the 4th Microquasars Workshop*, eds. Ph Durouchoux, Y. Fuchs and J. Rodriguez, (Kolkata, India: Centre for Space Physics)
- Sari, R., Piran, T., & Halpern, J.P. 1999, *ApJ*, 519, L17
- Smith, D., Remillard, R., Swank, J., Takeshima, T., & Smith, E. 1998, *IAU Circ.* 6855
- Taylor, G.B., Carilli, C.L., & Perley, R.A. 1999, *Synthesis Imaging in Radio Astronomy II* (San Francisco: Astronomical Society of the Pacific)
- Thé, P.S., de Winter, D., & Pérez, M.R. 1994, *A&AS*, 104, 315
- Thompson, A.R., Moran, J.M., & Swenson, G.W. 2001, *Interferometry and Synthesis in Radio Astronomy*, Second Edition (New York: Wiley Interscience)
- Ueda, Y., Ishida, M., Inoue, H., Dotani, T., Greiner, J., & Lewin, W.H.G. 1998, *ApJ*, 508, L167
- Wagner, R.M. & Starrfield, S.G. 1998, *IAU Circ.* 6857
- Wieringa, M.H., Kulkarni, S.R., & Frail, D.A. 1999, *A&AS*, 138, 467
- Woodsworth, A.W. & Hughes, V.A. 1977, *A&A*, 58, 105
- Wright, M., Dickel, J., Koralesky, B., & Rudnick, L. 1999, *ApJ*, 518, 284

This 2-column preprint was prepared with the AAS L^AT_EX macros v5.2.